An Fe-Rich Slag-Based Mortar for 3D Printing

Glenn Beersaerts[1(✉)], Sandra S. Lucas[2], and Yiannis Pontikes[1]

[1] Materials Engineering, KU Leuven, Leuven 3000, Belgium
glenn.beersaerts@kuleuven.be
[2] Built Environment, University of Technology Eindhoven, Eindhoven 5600, The Netherlands

Abstract. 3D printing can lead to a technological breakthrough in the construction sector. However, the sustainability aspect of 3D printing mortar can be disputable, as 3D printable mortar contains a high amount of ordinary Portland cement (OPC). The sustainability can be increased by replacing OPC with an Fe-rich slag, which originates from the metallurgical industry and is nowadays used for low-value applications. A mortar composition consisting mainly of slag and a small amount of OPC is called a hybrid mortar and is alkali-activated to ensure that the slag is participating in the binder formation. In this study, the amount of OPC is decreased significantly, down to 6 wt% and the slag content is increased up to 28 wt% over total solid content. This work investigated the effect of several components in the hybrid mixture on the early-age stiffness development, late-age shrinkage, creep and mechanical strength and is compared to a commercial OPC-based 3D printable mortar. The components, which are important to obtain a 3D printable mixture, comprise OPC, Si fume, fine limestone, superplasticizer and carbon fibres. This study shows that the additions significantly influence the stiffness and mechanical strength development of the hybrid. The shrinkage and creep behaviour of the hybrid was considerably lower compared to the benchmark material.

Keywords: Fe-rich slag · Alkali-activated materials · 3D-printing · Dynamic E-modulus · Shrinkage · Creep

1 Introduction

The construction sector is considered a low innovative sector compared to other industries [1]. Extrusion based 3D printing of construction elements can be a game-changer in the construction industry. New architectural features can be realized as 3D printing increases the freedom of movement [2, 3]. Further, 3D printing can offer several environmental and economic advantages compared to the traditional construction process. Using 3D printing can result in a decrease in construction errors, costs and a faster construction process with reduced labour cost and safety risks [4]. Currently, over 50% of the construction costs are allocated to the fabrication of formwork, which is not needed anymore when 3D printing.

The environmental aspect is, however, sometimes disputable. Ordinary Portland cement (OPC)-based 3D-printable mortars contain a significantly higher amount of OPC, from 10% up to 22% or more, compared to conventional high-performance OPC-based

F. P. Bos et al. (Eds.): DC 2020, RILEM Bookseries 28, pp. 3–12, 2020.
https://doi.org/10.1007/978-3-030-49916-7_1

mortars [5]. However, to produce 1 ton of OPC, around 0.8 ton of CO_2 is emitted, which implies that OPC is an environmentally unfriendly material [6, 7]. Research is performed on the use of precursors, alternative to OPC, for 3D printed applications in an attempt to reduce the environmental impact. Alkali-activated fly ash (FA) 3D printable mortars are mostly reported in the literature, with mechanical properties comparable to the conventional cast process [8]. Ground Granulated Blast Furnace slag (GGBFS) can be introduced in FA-based mortars as well to increase the mechanical strength [9]. Apart from the use of alternative precursors, several raw materials suitable for cementitious as well as alkali-activated materials are used to obtain a 3D printable mixture. Silica fume can be introduced to modify the mortar consistency in such a way that the desired yield stress and viscosity of the mixture can be obtained and the extrusion and mechanical performance are improved [9, 10]. Limestone can also be used to increase the number of interparticle contacts in the mixture and to improve extrudability and buildability [11]. The amount and type of superplasticizer (SP) are important as well, as it can influence the workability and buildability of the mixture, while fibres can improve the buildability and can reduce the shrinkage behaviour [12].

Apart from the use of GGBFS, other slags, which are not yet valorised to their full potential, can be used as well as alternative precursors. In detail, slags that originate from the Cu, Pb and Zn industry differ significantly, with respect to the chemistry, from GGBFS. These slags contain a high amount of Fe and are mostly used as a filler or are landfilled. Fe-rich slag can partially replace the OPC and can participate, after alkali-activation, in the binder formation. The binder formed from an alkali-activated OPC and Fe-rich slag blend is called a hybrid binder. The use of hybrid binders can reduce CO_2 emissions up to 80% compared to OPC-based binders, although numbers vary [13, 14]. Despite the strong environmental drive, a number of properties for both the fresh and hard hybrid mortar are not yet investigated.

In the work herein, different Fe-rich hybrid mortar formulations are produced which are intended for 3D printing. The different hybrid formulations are obtained by modifying the amount of several raw materials that are important for 3D printing. These raw materials comprise OPC, SP, silica fume, fine limestone and alkali-resistant carbon fibres. The effect of these components on the early and late-age properties of the mortar are investigated and compared to a commercially available OPC-based 3D printable mortar. The investigated early-age property comprises stiffness, and late-age properties are shrinkage, creep and flexural and compressive strength. A 1 M KOH activator is used in the hybrid formulations to enable the Fe-rich slag participation in the binder, without the loss of the SP effectiveness. Using an alkali-resistant SP is important to obtain suitable rheology for printing and to reduce the amount of activator, which impact the drying shrinkage.

2 Methodology

The precursors used in the mix formulation were CEMI 52.5 R (OPC) from CRH, an Fe-rich slag, originating from the Cu and Pb metallurgical industry, and fly-ash class F (FA) from Baumineral. The ultrafine materials comprise limestone (FL) powder (BETOFILL, Euroment) and silica fume (SF) from Elkem (microsilica 920). C-fibres

(CF) were introduced in the mixture as well. Quartz sand was used as aggregate. The crystalline composition of the Fe-rich slag was analysed by X-Ray Diffraction (D2 Phaser XRD, Bruker) measuring 2theta angles from 5° to 70° at a voltage of 30 kV and a current of 10 mA. The crystal phases and amorphous content were quantified on a blend composed of the slag and 10 wt% of a standard, crystalline ZnO, after milling in a McCrone micronizing mill while using hexane (>99% pure) and corundum beads as the milling media. The XRD pattern showed that the Fe-rich slag amorphous content ranged from 70 to 85 wt%, with wüstite (3–9 wt%), spinel (10–20 wt%) and quartz (0.1–1 wt%) being identified as the crystalline phases. The chemical bulk composition of the Fe-rich slag was determined by X-ray fluorescence (XRF, spectrometer PW 2400, Philips) and is shown in Table 1. The particle size distribution (PSD) of each raw material was determined by laser diffraction in wet conditions (Beckman Coulter LS 13 320). The PSD of each raw material is given in Table 2 and shows that SF has the smallest D_{50} (0.15 μm), followed by FL (5.7 μm), OPC (5.8 μm), Fe-rich slag (8.4 μm), FA (12.9 μm) and sand (544.2 μm). The specific density of the raw materials was measured by a pycnometer according to ASTM-B417-64 and is shown in Table 2. The specific density is the largest for the Fe-rich slag (3.4 g/cm^3), followed by the OPC, FL, FA, sand and finally SF.

Table 1. The bulk chemistry of the Fe-rich slag.

Element	FeO	SiO_2	CaO	Al_2O_3	Na_2O	MgO	Other
Range (wt%)	35-46	20-31	11-21	2-7	0.5-2.5	0.5-2.5	2-7

Table 2. The density and the D_{10}, D_{50} and D_{90} (μm) of each raw material.

Raw material	D_{10}	D_{50}	D_{90}	Specific density (g/cm^3)
Fe-rich slag	1.6	8.4	47.1	3.4
FA	1.4	12.9	54.2	2.6
OPC	0.9	5.8	16.8	3.1
FL	1.0	5.7	16.8	2.7
SF	0.1	0.2	0.5	2.2
Sand	348.5	544.2	790.2	2.5

The precursors were alkali-activated with a 1 M KOH alkali solution. The 1 M KOH solution was produced at least 24 h prior mixing, by dissolving KOH pellets (98% pure, Sigma Aldrich) in tab water. To lower the liquid content, two additives, a MasterGlenium 65 Con superplasticizer (SP) from BASF and bassanite (99% pure, Sigma Aldrich), were used. Prior to the mortar preparation, the superplasticizer and bassanite were introduced in the alkali solution and mixed for 30 s at low speed (130 rpm). Afterwards, the precursors and ultrafine materials were gradually added for 1 min and mixed for another minute at low speed. When C-fibres were used, the fibres were introduced during the paste preparation. Finally, the sand was added for 1 min to

the mixture and the blend was mixed for another min at high speed (220 rpm). In this research, the amounts of CEMI 52.5 R (OPC), superplasticizer (SP), silica fume (SF), fine limestone (FL) and C-fibres (CF) were modified, while the amount of sand, fly ash (FA) and Fe-rich slag remained approximately constant for each formulation. The mix composition and the bulk density of the hardened samples is shown in Table 3, in which the benchmark corresponds to the commercial 3D printable mortar and M to the hybrid mix developed herein.

Table 3. The investigated mixtures with its raw materials and bulk density.

Raw material	Bulk density (kg/m^3)	OPC	Slag + FA	SF	FL	Sand	Additives	AS	CF
Benchmark	2065	/	/	/	/	/	/	/	/
M1	2160	145	742	77	77	1157	17	185	0
M2DSP	2225	145	744	77	77	1160	13	186	0
M3IFL	2264	141	724	75	141	1128	17	181	0
M4ISF	2262	140	720	140	75	1122	18	179	0
M5DOPC	2260	72	821	77	77	1158	16	185	0
M6ICF	2185	144	738	76	76	1150	19	184	9

For identifying the dynamic E-modulus in all mixtures, an ultrasonic pulse velocity test (Type IP8, UltraTest) was employed, which continuously monitored the velocity of P-waves through the sample. The fresh mortar was cast in a cylindric silicone mould, with an emitter on one side emitting a P-wave every 10 s, and a receiver on the opposite site measuring the time delay of the wave that travelled through the sample. From this time delay, the dynamic E-modulus (E-mod) was calculated, with the formula $E_{dyn}(t) = k\ v(t)^2 \rho$ with $k = 0.876$, which gives an indication for the stiffness. The ultrasonic measurement was initiated 8 min after mixing and lasted up to 24 h.

The fresh mixtures were cast in $4 \times 4 \times 16$ cm^3 moulds and sealed for 24 h at room temperature. Afterward, the samples were demoulded and exposed to 20 °C and 65% relative humidity for 28 days. Once demoulded, two metallic pins were placed on the two long side faces of each sample and the initial distance was measured. At specific times, the length difference or displacement was measured for each sample. In this way, the effect of the mixture composition on the displacement behaviour can be identified. Two samples of each mixture were subjected to a vertical load of 15 kN after 9 days of curing to measure the total creep. 9 days of curing were necessary for the samples to develop enough strength in order to apply a load on the samples. The load was applied to the samples for 19 days and the deformation of the samples was measured at specific times. From the measured total deformation, the shrinkage is deducted and divided by the load stress (11.25 MPa) to obtain the specific creep. The 2, 7 and 28 days flexural and compressive strength of each sample were tested according to EN 196-1. Two replicates were made for each mixture to investigate the variation in displacement behaviour and mechanical strength.

3 Results and Discussion

The benchmark exhibited a steady increase in E-mod (Fig. 1) from the start of the measurement. After 2 h, the gradient in E-mod changed, from a steady to an exponential increase, which could be related to the hardening process of the material. At that moment, a rigid network structure is formed due to the hydration process. M1 measured a slow increase in E-mod, which was insignificant during the first 2 h. In mixture M1, the use of SP in excess could delay reactivity, as the SP is able to change the surface interactions of the cement particles. The early-age E-mod development is accelerated when the amount of OPC (M5DOPC) or the amount of SP (M2DSP) is decreased. In both cases, the increase in E-mod can be explained by the decreased effect of the SP. The SP is effective on the cement and ettringite surface area and when the amount of SP decreased (M2DSP), the potential for particles to agglomerate is increased [15] and less free water is available. When the amount of OPC decreased (M5DOPC) less ettringite is formed, and consequently less surface area is available for the SP to adsorb on. At a later age, from 8 h, the E-mod gradient is decreased, as less OPC was available and thus fewer hydration reactions were taking place to contribute to the binder formation. M2DSP shows at a later age an increase in the E-mod gradient compared to M1 because less SP was available to delay the reactivity. Increasing the amount of FL (M3IFL) did not influence the E-mod during the 1st h post mixing. After 1 h, however, the E-mod developed much faster compared to M1, following a similar trend as the benchmark for 2 h long. Adding FL increased the specific surface area and could act as nucleation sites. In this way, the precipitation process is accelerated and a mixture of fines in between the coarser slag particles could result in the formation of a stiffer initial network structure. The introduction of other fines, such as SF (M6ISF), accelerated the E-mod development even faster, resulting in an early-age stiffness increase comparable to the benchmark. The alkali solution could dissolve part of the SF and could form an initial silicate network which increased the stiffness and decreased the setting time [16]. The introduction of CF in the mixture (M6ICF) significantly increased the E-mod, in particular at an early-age, which was higher compared to the benchmark. Adding CF resulted in an entangled structure in the mixture, causing an increase in stiffness.

The mixtures investigated in the current research exhibited a negative displacement, which implies that the samples are shrinking (Fig. 2). The benchmark exhibited a shrinkage up to 1180 μm/m after 28 days. This high shrinkage might be explained by the lower sand fraction in the benchmark, resulting in a less aggregate supported matrix and a higher binder content [17]. The hybrid samples demonstrated much lower shrinkage values, ranging from 491 to 800 μm/m after 28 days. The hybrid samples evolved after 14 days to a plateau value, while the benchmark sample continued to shrink. M2DSP shows an increase in shrinkage with 30% (645 μm/m) compared to M1. The latter can be explained by the fact that SPs are generally known to reduce the shrinkage because they decrease the surface tension in the pores [18]. When a SP is used, less water is needed to cover the cement surface and more water is free. If more water is physically bonded on the cement surface and, at a later age in the binder micropores, a higher capillary tension is generated to evaporate the water. Consequently, decreasing the SP increased the

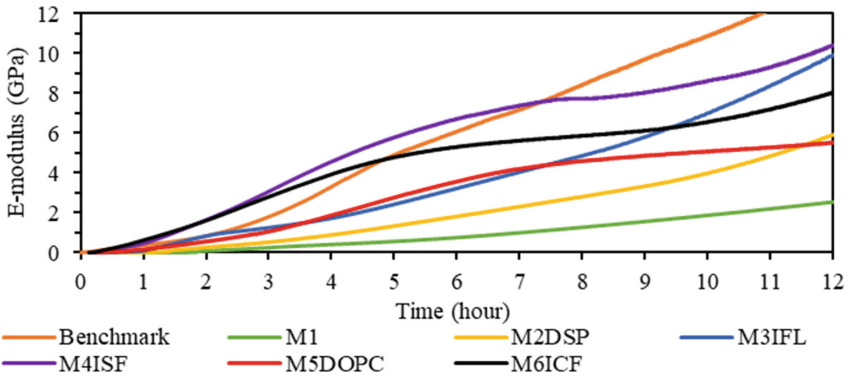

Fig. 1. The E-mod development of all mixtures from min 8 to 12 h post mixing.

shrinkage. M3IFL shows a shrinkage behaviour similar to M2DSP and is increased with 22% (594 µm/m) compared to M1. The increase in FL resulted in an increase in the surface area that needs to be covered by water. In this way, smaller pores are formed in which water is situated and consequently higher capillary tension is generated, resulting in a higher shrinkage. M4ISF measured a slight increase in shrinkage of 11% and is considered not significant. Decreasing the amount of OPC (M5DOPC) did not significantly influence the shrinkage behaviour (546 µm/m), compared to M1 (491 µm/m). The introduction of CF to the mixture (M6ICF) increased the shrinkage with 51% compared to M1, to a value of 744 µm/m. Depending on the amount and type of fibres, the fibre addition can have a negative effect on the shrinkage. The introduction of fibres can lead to an inhomogeneous mixture which can affect the shrinkage behaviour. The effect of fibre addition in hybrid binders should be investigated in the future.

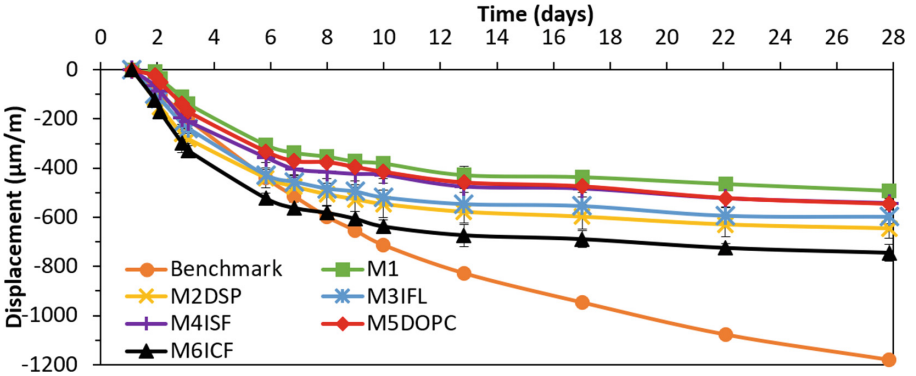

Fig. 2. The displacement of all investigated mixtures for 28 d long.

The benchmark shows the highest deformation creep, up to −92(µm/m)/MPa at 28 days (Fig. 3). The hybrid mixtures evolved towards a plateau after 28 days, while the benchmark continued to shrink. The hybrid samples show a creep which is higher for the first 2 days compared to the benchmark. The difference in creep can be explained by the higher paste to aggregate ratio in the benchmark. M1 shows the highest creep (−60(µm/m)/MPa) for the hybrid samples followed by M5DOPC (−44(µm/m)/MPa). In Fig. 3 it is visible that increasing the amount of FL and SF reduced the creep. M3IFL and M4ISF show a similar creep (−34(µm/m)/MPa), which is decreased with 45% compared to M1. Increasing the amount of fines or surface area improved the binder resistance to deformation when subjected to a force. It is visible in Fig. 3 that the introduction of CF reduced significantly (M6ICF) the creep at an early and late age. Fibres in the sample resulted in the formation of a rigid monolith, more resistant to deformation [19]. M2DSP shows a similar creep behaviour as M6ICF, implying that a decrease in SP resulted in a stronger binder, less subjected to deformation.

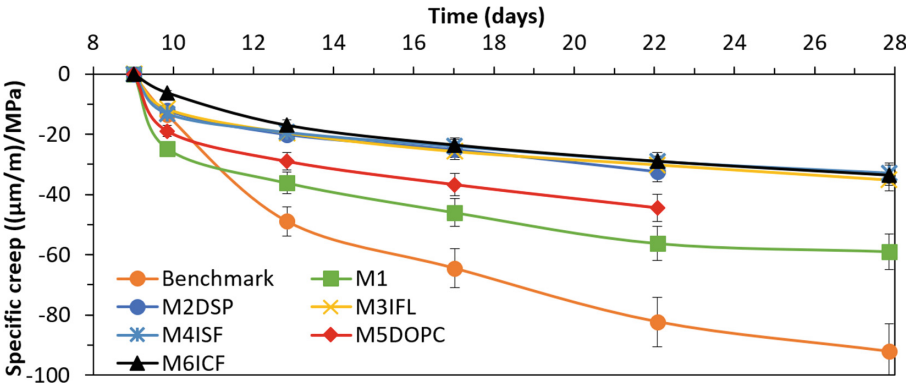

Fig. 3. The specific creep from day 9 till day 28 for all mixtures.

The 2, 7 and 28 days flexural strength of all samples are presented in Fig. 4a and show that the benchmark has a significant strength increase between 2 and 7 days (8.6 MPa). M1 shows a 28 days flexural strength of 4.9 MPa, which is almost half of the benchmark. Decreasing the SP (M2DSP) increased the flexural strength with 48%, due to the increased reactivity. Increasing the amount of FL (M3IFL) or SF (M4ISF) in the mixture increased the 2, 7 and 28 days flexural strength, with a 28 days increase of 65% and 44%, respectively. M5DOPC measured a lower flexural strength compared to M1, as less OPC is available to develop a strong binder. M6ICF obtained the highest flexural strength, and compared to M1, a 2, 7 and 28 days flexural strength increase of 51%, 71% and 83%, correspondingly. These results state that fibres increased the flexural strength properties of hybrid samples. The benchmark has the highest 2 days compressive strength (29.5 MPa) compared to all other hybrid samples (Fig. 4b). Decreasing the SP increased the 2, 7 and 28 days compressive strength properties, compared to M1, by 22%, 28% and 31%, respectively. Increasing the amount of FL (M3IFL) and SF (M4ISF) improved the 2, 7 and 28 days compressive strength by

around 40%. The addition of fines offered additional nucleation sites and improved the interparticle filling leading to reduced number of pores and improved mechanical properties [20, 21]. Decreasing the amount of OPC, resulted in a decrease in compressive strength with 25% (M5DOPC). The introduction of CF improved the 2, 7, and 28 days compressive strength with 44%, 50% and 63%, respectively.

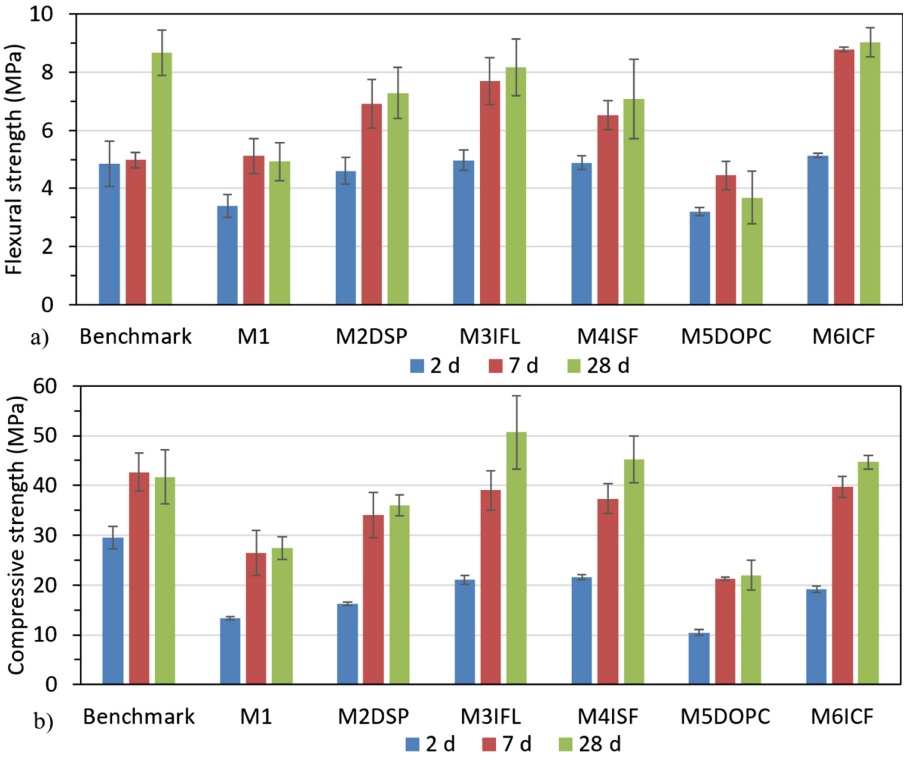

Fig. 4. (a) Shows the flexural strength, and (b) shows the compressive strength of each mixture at 2, 7 and 28 days.

4 Conclusion

In the current research, the early and late-age properties of different hybrid mortars, originating from alkali-activated Fe-rich slag were investigated and compared with a commercial 3D printable OPC-based mixture. The proportion of several raw materials in the hybrid mixture, which are important to improve the printing process, was the main experimental parameter in this study. The early-age stiffness of the commercial mixture outperformed the hybrid mixture developed herein. The shrinkage and creep of the commercial 3D printable mixture, however, was consistently higher compared to the hybrid one. The rate in dynamic E-modulus development was increased when decreasing the amount of superplasticizer. The decrease in superplasticizer had an important effect on

the late-age properties, as it increased the shrinkage with 30%, decreased the creep with 45% and increased the flexural and compressive strength with 48% and 31%, respectively. The increase in silica fume resulted in a hybrid mixture with an early-age structural build-up. Fine limestone and silica fume offered more precipitation sites to develop a stronger binder which resulted in an increase in flexural and compressive strength of around 40% and a decrease in creep of 45% for both. The amount of OPC in the hybrid mixtures can influence the effectiveness of the superplasticizer and mechanical properties. Decreasing the amount of OPC resulted in a decreased plasticizing effect and consequently an earlier dynamic E-modulus development. However, when less cement was available, a weaker binder was formed which negatively affected the mechanical properties. The addition of carbon fibres resulted in the development of a high early-age dynamic E-modulus. Carbon fibres significantly increased the flexural and compressive strength, by 83% and 63%, respectively, and decreased the creep by 45%. Carbon fibres seemed to increase the shrinkage, a behaviour that should be further investigated. This study demonstrated that hybrid binders, originating mainly from Fe-rich slags, reached suitable late-age properties, although the early-age properties still can be improved.

Acknowledgements. The authors would like to thank B. Rijssen and M. Suijs for their support in performing the measurements. This research has received financial support of the Center for Research, Recovery, and Recycling (https://wp.wpi.edu/cr3/).

References

1. Barbosa, F., Woetzel, J., Mischke, J., Ribeirinho, M.J., Sridhar, M., Parsons, M.: Reinventing Construction: A Route to Higher Productivity. McKinsey Global Institute (2017)
2. Sai Sandeep, U., Muralidhara Rao, T.: A review on 3D printing of concrete-the future of sustainable construction. J. Civ. Eng. **7**(3), 49–62 (2017)
3. Kothman, I., Faber, N.: How 3D printing technology changes the rules of the game. J. Manuf. Technol. Manage. **27**(7), 932–943 (2016)
4. Bos, F., Wolfs, R., Ahmed, Z., Salet, T.: Additive manufacturing of concrete in construction: potentials and challenges of 3D concrete printing. Virtual Phys. Prototyping **11**(3), 209–225 (2016)
5. Chen, Y., Copuroglu, O., Veer, F.: A critical review of 3D concrete printing as a low CO_2 concrete approach. Heron **62**(3), 1–23 (2017)
6. Li, C., Gong, X.Z., Cui, S.P., Wang, Z.H., Zheng, Y., Chi, B.C.: CO_2 emissions due to cement manufacture. Mater. Sci. Forum **685**, 181–187 (2011)
7. Hendriks, C.A., Worrell, E., Price, L., Martin, N., Ozawa Meida, L., Jager, D.: Emission reduction of greenhouse gases from the cement industry. In: Materials Science, pp. 939–944 (2003)
8. Panda, B., Paul, S.C., Hui, L.J., Tay, Y.W.D., Tan, M.J.: Additive manufacturing of geopolymer for sustainable built environment. J. Clean. Prod. **167**, 281–288 (2017)
9. Panda, B., Unluer, C., Tan, M.J.: Investigation of the rheology and strength of geopolymer mixtures for extrusion-based 3D printing. Cement Concr. Compos. **94**, 307–314 (2018)
10. Kazemian, A., Yuan, X., Cochran, E., Khoshnevis, B.: Cementitious materials for construction-scale 3D printing: laboratory testing of fresh printing mixture. Constr. Build. Mater. **145**, 639–647 (2017)

11. Alghamdi, H., Nair, S.A.O., Neithalath, N.: Insights into material design, extrusion rheology, and properties of 3D-printable alkali-activated fly ash-based binders. Mater. Des. **167**, 107634–107647 (2019)
12. Le, T.T., Austin, S.A., Lim, S., Buswell, R.A., Gibb, A.G.F., Thorpe, T.: Mix design and fresh properties for high-performance printing concrete. Mater. Struct. **45**(8), 1221–1232 (2012)
13. Turner, L.K., Collins, F.G.: Carbon dioxide equivalent (CO2-e) emissions: a comparison between geopolymer and OPC cement concrete. Constr. Build. Mater. **43**, 125–130 (2013)
14. van Deventer, J.S.J., Provis, J.L., Duxson, P., Brice, D.G.: Chemical research and climate change as drivers in the commercial adoption of alkali activated materials. Waste Biomass Valorisation **1**(1), 145–155 (2010)
15. Ferrari, L., Kaufmann, J., Winnefeld, F., Plank, J.: Interaction of cement model systems with superplasticizers investigated by atomic force microscopy, zeta potential, and adsorption measurements. J. Colloid Interface Sci. **347**(1), 15–24 (2010)
16. Siddique, R., Khan, M.I.: Supplementary Cementing Materials. Springer, Berlin (2011)
17. Rao, G.A.: Long-term drying shrinkage of mortar—influence of silica fume and size of fine aggregate. Cem. Concr. Res. **31**(2), 171–175 (2001)
18. Qian, C., Zhang, Y., Huang, H., Qu, J., Guo, J.: Influences of superplasticizers on the basic and drying creep of concrete. Struct. Concr. **17**(5), 729–735 (2016)
19. Song, W., Yi, J., Wu, H., He, X., Song, Q., Yin, J.: Effect of carbon fiber on mechanical properties and dimensional stability of concrete incorporated with granulated-blast furnace slag. J. Clean. Prod. **238**(117819), 1–11 (2019)
20. Xiang, J., Liu, L., Cui, X., He, Y., Zheng, G., Shi, C.: Effect of limestone on rheological, shrinkage and mechanical properties of alkali – activated slag/fly ash grouting materials. Constr. Build. Mater. **191**, 1285–1292 (2018)
21. Rostami, M., Behfarnia, K.: The effect of silica fume on durability of alkali activated slag concrete. Constr. Build. Mater. **134**, 262–268 (2017)